RESEARCH ARTICLE

The orbitofrontal cortex represents advantageous choice in the Iowa gambling task

Rujing Zha[1] 🟢 | Peng Li[2] | Ying Liu[1] | Abdulqawi Alarefi[1] |
Xiaochu Zhang[1,3,4,5] 🟢 | Jun Li[6]

[1]Department of Radiology, the First Affiliated Hospital of USTC, Department of Psychology, School of Humanities & Social Science, Division of Life Science and Medicine, University of Science & Technology of China, Hefei, Anhui, China

[2]Department of Automation, School of Information Science and Technology, University of Science and Technology of China, Hefei, Anhui, China

[3]Application Technology Center of Physical Therapy to Brain Disorders, Institute of Advanced Technology, University of Science & Technology of China, Hefei, Anhui, China

[4]Hefei Medical Research Center on Alcohol Addiction, Affiliated Psychological Hospital of Anhui Medical University, Hefei Fourth People's Hospital, Anhui Mental Health Center, Hefei, Anhui, China

[5]Biomedical Sciences and Health Laboratory of Anhui Province, University of Science & Technology of China, Hefei, Anhui, China

[6]Department of Automation, University of Science and Technology of China, Hefei, China

Correspondence
Jun Li, Department of Automation, University of Science and Technology of China, Hefei 230027, China.
Email: ljun@ustc.edu.cn

Xiaochu Zhang, Key Laboratory of Brain Function and Disease, Chinese Academy of Sciences, School of Life Sciences, University of Science & Technology of China, Hefei, Anhui 230027, China.
Email: zxcustc@ustc.edu.cn

Abstract

A good-based model, the central neurobiological model of economic decision-making, proposes that the orbitofrontal cortex (OFC) represents binary choice outcome, that is, the chosen good. A good is defined by a group of determinants characterizing the conditions in which the commodity is offered, including commodity type, cost, risk, time delay, and ambiguity. Previous studies have found that the OFC represents the binary choice outcome in decision-making tasks involving commodity type, cost, risk, and delay. Real-life decisions are often complex and involve uncertainty, rewards, and penalties; however, whether the OFC represents binary choice outcomes in a complex decision-making situation, for example, Iowa gambling task (IGT), remains unclear. Here, we propose that the OFC represents binary choice outcome, that is, advantageous choice versus disadvantageous choice, in the IGT. We propose two hypotheses: first, the activity pattern in the human OFC represents an advantageous choice; and second, choice induces an OFC-related functional network. Using functional magnetic resonance imaging and advanced machine-learning tools, we found that the OFC represented an advantageous choice in the IGT. The OFC representation of advantageous choice was related to decision-making performance. Choice modulated the functional connectivity between the OFC and the superior medial gyrus. In conclusion, the OFC represents an advantageous choice during the IGT. In the framework of a good-based model, the results extend the role of the OFC to complex decision-making situation when making a binary choice.

KEYWORDS
advantageous choice, fMRI, multivoxel pattern analysis, orbitofrontal cortex, psycho-physiological interaction

1 | INTRODUCTION

The identified neurobiological mechanism underlying economic decision-making includes a valuation stage and a choice stage (Hunt et al., 2014; Kable & Glimcher, 2009; Rodriguez et al., 2014). Decision makers evaluate the subjective values and characteristics of available options in the valuation stage. However, encoding subjective value and characteristics is not sufficient for making decisions, and one of the available options still needs to be chosen by decision makers at the choice stage (Hunt et al., 2014; Kable & Glimcher, 2009; Rodriguez et al., 2014). At this stage, a good-based model, a central neurobiological model of economic decision-making, proposes that the orbitofrontal cortex (OFC) represents the binary choice outcome, that is, the chosen good (Padoa-Schioppa, 2011). A good is defined by a group of determinants characterizing the conditions in which the commodity is offered, which can include commodity type, time delay, cost, risk, and ambiguity (Padoa-Schioppa, 2011).

Consistent with a good-based model, previous studies have found that the OFC represents the binary choice outcome in juice-choice tasks (Padoa-Schioppa & Assad, 2006) and decision-making tasks involving costs (Cai & Padoa-Schioppa, 2019), risks (Raghuraman & Padoa-Schioppa, 2014), and delays (Chen et al., 2019). For example, different OFC neurons respond when a monkey chooses between different juice types (Padoa-Schioppa & Assad, 2006). Some OFC neuronal responses in monkeys encode choosing a high-cost option versus choosing a low-cost option (Cai & Padoa-Schioppa, 2019). Some other OFC neurons in monkeys encode choosing a risky option versus choosing a nonrisky option (Raghuraman & Padoa-Schioppa, 2014). The OFC activity pattern in the human brain can classify choosing smaller-but-immediate options versus choosing larger-but-delayed options (Chen et al., 2019). Animal studies with OFC lesion and reversible inactivation have been implicated in risky decision-making in animals (Rivalan et al., 2011; St Onge & Floresco, 2010; Zeeb & Winstanley, 2011, 2013). However, real-life decisions are often complex and involve uncertainty, rewards, and penalties.

The inability to make choices in a complex decision-making situation, for example, Iowa gambling task (IGT), is a symptom of several brain disorders, including borderline personality disorder (Linhartová et al., 2020), attention-deficit/hyperactivity disorder (Linhartová et al., 2020), anorexia nervosa (Verharen et al., 2019), addiction (Kluwe-Schiavon et al., 2020), obsessive-compulsive disorder (Nisticò et al., 2021), and schizophrenia (Betz et al., 2019). In the IGT, reward value is a key decision-making parameter (Bechara et al., 1997).

Whether the OFC represents a binary choice outcome in the IGT, advantageous choice (i.e., choosing an option with a high reward value) versus disadvantageous choice (i.e., choosing an option with a low reward value), remains unclear. The meaning of OFC representing an advantageous choice in the IGT means that activity pattern in the OFC differed between advantageous and disadvantageous choices in the IGT.

It is worth noting that the OFC represents a cytoarchitectonic and functionally heterogeneous region (Rolls, 2021; Wallis, 2011). The medial OFC includes architectonic areas 13 and 11 and the lateral OFC includes architectonic area 12 (Rolls, 2021). The medial OFC has functional connectivity with the parahippocampal gyrus, the hippocampus, the insula, the cingulate cortex, the temporal gyrus, and the fusiform gyrus; while the lateral OFC has functional connectivity with the inferior frontal gyrus, the angular gyrus, and supramarginal gyrus (Du et al., 2020). Direct connections have been studied with diffusion tractography imaging (Heather Hsu et al., 2020). Specifically, the medial OFC has direct connections with the pregenual and subgenual parts of the anterior cingulate cortex. The lateral OFC has direct connections with the supracallosal anterior cingulate cortex, the inferior parietal cortex, the supramarginal gyrus, and some premotor cortical areas. Although both medial and lateral OFC have been involved in subjective value (Lopez-Persem et al., 2020; Suzuki et al., 2017), only the lateral OFC represents the elemental nutritive attributes of food (Suzuki et al., 2017). Rolls (2021) has reviewed that the human medial OFC represents reward value, and the lateral OFC represents punishments and nonreward (Rolls, 2021). Stalnaker et al. (2015) have reviewed a number of ideas about OFC functions, such as cognitive map, value, credit assignment, prediction errors, somatic markers, and response inhibition (Stalnaker et al., 2015). Recently, the OFC has been considered to be required for representing task structure (Zhou et al., 2021).

A line of studies has implicated the OFC at the valuation stage, that is, evaluating available options such as the value (Ballesta et al., 2020; Malvaez et al., 2019; Stuphorn, 2020; Yamada et al., 2018), risk (Burke & Tobler, 2011; Orsini et al., 2015; Payzan-LeNestour et al., 2013; Preuschoff et al., 2008), ambiguity (Hsu et al., 2005; Levy et al., 2010), and environmental statistics (Vertechi et al., 2020). For example, Hare et al. (2009) and Kable and Glimcher (2007) reported that OFC activity was correlated with high values versus low values. Kahnt (2018) has shown that the OFC represents the value of rewards independent of reward category and reward identity (Kahnt, 2018). Moreover, dopamine D2-receptor

blockade enhances decoding of reward in the OFC (Kahnt et al., 2015). Both Bartra et al. (2013) and Clithero and Rangel (2014) have shown that the OFC is a key brain area related to high subjective values versus low subjective values of different types of rewards using meta-analysis. Some studies have also investigated the neural basis of high ambiguity versus low ambiguity in complex decision-making. For example, Levy et al. (2010) showed that OFC activity is correlated with ambiguity level. Hsu et al. (2005) also revealed that the OFC showed greater activation in response to the level of ambiguity. Therefore, these studies have implicated the OFC in evaluating risk, ambiguity, and value.

A good-based model has proposed the OFC represents the choice in economic decision-making. Studies have shown that the OFC represents the choice in a juice-choice task (Padoa-Schioppa & Assad, 2006), decision-making tasks involving costs (Cai & Padoa-Schioppa, 2019), risks (Raghuraman & Padoa-Schioppa, 2014), and delays (Chen et al., 2019). However, several neurobiological studies investigated advantageous versus disadvantageous choice in the IGT and showed that blood oxygenation level-dependent (BOLD) activation using individual voxel-based methods in the OFC was not significantly associated with advantageous choice versus disadvantageous choice (Brevers et al., 2016; Christakou et al., 2009; Ding et al., 2017; Fukui et al., 2005; Jollant et al., 2010; Lawrence et al., 2009; Lin et al., 2008; Ma et al., 2015; Power et al., 2012; Tanabe et al., 2007; Werner et al., 2013). For example, Brevers et al. (2016) did not find any advantageous choice-related activation in the OFC in healthy controls or poker gamblers in the IGT.

The finding that the OFC was not implicated in advantageous choice versus disadvantageous choice in the IGT in these studies may be explained by the complex neurobiological architecture of the OFC. The firing of neurons in the OFC shows a heterogeneous relationship to reward parameters (Kahnt, 2018). Both decreasing and increasing responses to increases in reward value, size, and probability have been observed in the rodent and primate prefrontal cortex (Kennerley et al., 2009; Padoa-Schioppa & Assad, 2006; Schoenbaum et al., 1998). These "increasing" and "decreasing" neurons are not large-scale clustering in the OFC (Morrison & Salzman, 2011). This heterogeneous coding of reward may average out the signal of interest in individual fMRI voxels (Kennerley et al., 2009). Unlike the individual voxel-based method, the multivoxel pattern analysis (MVPA) can identify brain regions where overlapping neuronal populations encode the same event with opposite encoding schemes (Kahnt, 2018). For example, Kahnt et al. (2015) have used both MVPA and individual voxel-based methods to detect the effects of amisulpride on the OFC and found that the amisulpride changed activity pattern in the OFC without changing the mean signal between conditions (Kahnt et al., 2015). Moreover, multiple voxels activity pattern in the OFC represents delayed choice versus immediate choice in decision-making involving delays (Chen et al., 2019). Thus, we hypothesized that multiple voxels activity pattern in the OFC, especially medial OFC, would represent advantageous choice versus disadvantageous choice in the IGT.
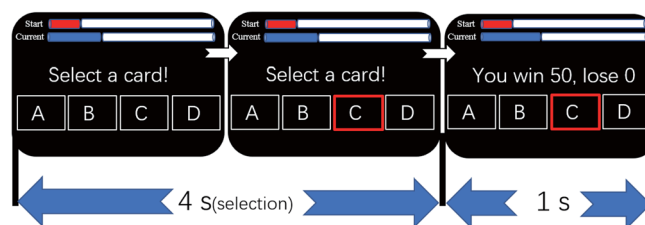

FIGURE 1 Experimental paradigm of the Iowa gambling task. Experimental paradigm of the Iowa gambling task. There were two phases for each trial. Four decks were presented in the first phase. Participants selected a card within 4 s in this phase (selection phase, 4 s); then, the outcome, including gain and loss, was presented in the second phase (feedback phase, 1 s)

Studies have shown that the superior medial gyrus is significantly activated during the contrast disadvantageous choice versus advantageous choices in the IGT (Ding et al., 2017; Fukui et al., 2005; Lawrence et al., 2009) and that the superior medial gyrus is also significantly activated during the contrast difficult decisions versus easy decisions in the delay discounting task (Zha et al., 2022). Moreover, the OFC shows functional connectivity with the superior medial gyrus in a decision-making task involving risk (McCormick & Telzer, 2017). We, therefore, hypothesized that the OFC would be functionally connected with the superior medial gyrus for choice.

2 | MATERIALS AND METHODS

2.1 | Participants

Fifty-five healthy participants were recruited in the study, and one participant was excluded after presenting with significant head motion (>3.0 mm) during functional magnetic resonance imaging (fMRI) scanning. The remaining 54 participants included 45 males and nine females (age: mean, 22.7 years; standard deviation (SD), 2.1 years; range, 19–27 years; education: mean, 16.3 years; SD, 1.8 years; range, 13–19 years). All participants recruited in the present research were right-handed. All participants were free of psychiatric or neurological history and had normal or corrected-to-normal vision. The study was approved by the Human Research Ethics Committee of the University of Science and Technology of China. The methods and procedures used in this study were carried out in accordance with the approved guidelines. Written informed consent was obtained from all participants before the study, consistent with the Declaration of Helsinki guidelines.

2.2 | Task paradigm

In the present study, we used the IGT (Bechara et al., 1997; Figure 1), a popular decision-making task for indexing real-life complex decision-

making. In each trial, the participants selected a card from among four decks of cards. The four decks were labeled A, B, C, and D as presented from left to right. For each participant, deck A, B, C, and D could be chosen by button press from the left middle finger, left index finger, right index finger, and right middle finger, respectively. On each card, there were different numbers of gain and possible loss points, and the participant received the net (gain–loss) points for choosing that card. Participants did not know the expected reward and variability in the outcomes for all decks before engaging in the task. In the task, the participants were asked to maximize the points they gained. Specifically, for each selection from deck A or B ("low reward value decks"), participants would gain 100 points, but the losses were organized so that over 10 selections from the decks, the participants would have an overall loss of 250 points. Specifically, deck A provided -150, -200, -250, -300, and -350 (loss) points every 10 selections, whereas deck B provided -1250 (loss) points in one out of 10 selections. For each selection from deck C or D ("high reward value decks"), the participants would win 50 points, and the losses were organized so that if participants made over 10 selections from these decks, they would obtain an overall profit of 250 points. The two decks differed in the frequency and magnitude of the punishment. Similar to the previous two decks, deck C provided -25, -40, -50, -60, and -75 (loss) points every 10 selections, whereas deck D provided -250 (loss) points once every 10 selections. Decks A and B had negative reward expectations and were operationally defined as having a low reward value. In contrast, decks C and D had positive reward expectations and were defined as having a high reward value. Therefore, choosing decks C and D was an advantageous choice, and choosing decks A and B was a disadvantageous choice. Similar to previous studies (Wang et al., 2017; Wei et al., 2018), the IGT was extended to 180 trials from the original 100 trials to facilitate rule learning (Bechara et al., 1997). The IGT consisted of three scan runs, with three blocks for each scan run and 20 trials for each block. The participants who had positive net winnings at the end of the task would obtain extra money (10¥/1000 points). The final net winnings were defined as the total score.

2.3 | Behavioral analysis—Reinforcement learning model

This procedure followed that of a previous study (Wei et al., 2018). The reinforcement learning model (Behrens et al., 2007) was adapted to analyze the behavioral data. Reward prediction errors (RPEs) were included in the model, according to the suggestion by Sutton and Barto (1998). An RPE (δ_t) was defined as the difference between the actual reward r_t and the predicted reward $\widehat{v}_t$ at trial t. The formula for this definition was as follows:

$$\delta_t = r_t - \widehat{v}_t. \tag{1}$$

The RPE was used to update reward prediction in the model using the following formula:

$$\widehat{v}_{t+1} = \widehat{v}_t + \alpha \cdot \delta_t. \tag{2}$$

where α is the learning rate for the RPE in the update formula (Behrens et al., 2007). Then, maximum likelihood estimation (MLE) was adopted to estimate the learning rate based on the samples. Here, π_{it} was defined as the probability of choice i at trial t. We transformed the data with an exponential function when we calculated the value of π_{it} using the following formula:

$$\pi_{it} = \frac{e^{\widehat{v}_{it}}}{\sum_{j=1}^{n} e^{\widehat{v}_{jt}}}. \tag{3}$$

The learning rate was estimated separately by maximizing the likelihood function for each participant:

$$\text{Maximum log} - \text{likelihood} = \max \sum_{t=1}^{M} \log \pi_{i_t,t} \tag{4}$$

where i_t represents the deck selected at trial t, $i_t \in \{1,2,3,4\}$, and $\pi_{i_t,t}$ represents the probability of selecting deck i_t at trial t.

Cohen's d values were calculated via G*Power 3.1 software (Faul et al., 2007). We calculated the total net good decks, which was the number of advantageous choices minus the number of disadvantageous choices in 180 trials.

2.4 | fMRI data acquisition and preprocessing

Gradient echo-planar imaging data were acquired using a 3.0T, 8-channel head coil Trio scanner (Siemens Medical Solution, Erlangen, Germany) with a circularly polarized head coil in Hefei. We restrained head motion with foam padding. A T2*-weighted echo-planar imaging sequence (FOV $=$ 240 mm, TE $=$ 30 ms, TR $=$ 2000 ms, flip angle $=$ 85° matrix $=$ 64 $\times$ 64) with 33 axial slices (no gaps, 3.7 mm thick) covering the whole brain was used to acquire the functional MR images. There were three runs of IGT, each of which contained 210 epochs. Furthermore, high-resolution T1-weighted spin-echo imaging data (1 mm isotropic voxel) were also acquired for anatomical overlay.

We preprocessed the imaging following the workflows proposed in a previous article (Esteban et al., 2019). All functional MR images were preprocessed using Analysis of Functional Neuroimages (Version AFNI_18.2.03) software (Cox, 1996). All fMRI data were corrected for temporal shifts between slices and motion and grand-mean scaled. We used rigid-body transformations to calculate the head motion in the IGT task during fMRI data. This method assumes that the size and shape of the registered images are the same and only differ in translations along the x, y, and z axes, and three rotation angles (roll, pitch, and yaw). The motion correction was performed by AFNI's 3dvolreg (Cox, 1996). Low-frequency signal drifts were filtered using a cutoff of 128 s. Volumes meeting the following criteria were removed: translation >0.3 mm or rotation >0.3° between consecutive volumes (Rose et al., 2012). Siegel et al. (2014) have shown that motion censoring

performed well in general linear models with HRF response shapes and have concluded that motion censoring improves the quality of task-based fMRI data and can be a valuable data processing procedure in task-based fMRI studies (Siegel et al., 2014). This motion censoring procedure has been popularly used in studies with task-based fMRI data to mitigate motion effects (Kirwan et al., 2009; Rose et al., 2012; Stark et al., 2010). For each run, we dropped the first two volumes to enhance stability. Linear regression was also performed to remove linear trends. All functional volumes were non-linearly transformed to MNI space (resampled voxel size: $4 \times 4 \times 4$ mm^3) according to the spatial transformation between the anatomical data and the MNI space. Volumes were spatially smoothed with a Gaussian kernel (full-width at half-maximum = 8 mm) and were used for general linear model and psycho-physiological interaction (PPI) analysis. Unsmoothed data were used for MVPA.

2.5 | General linear model for value signals

To illustrate the neural activations of the values, including RPE, gain, loss, and reward predictions for the four decks, a general linear model was used to examine the BOLD signals in which brain regions were correlated with these values. The general linear model was run for each value and included (1) an interest regressor, that is, one-value regressor, defined as RPE, gain, loss, or reward prediction for the four decks during the epochs when feedback was presented and 0 for other epochs, and (2) six noninterest regressors for head motion. We specified seven first level models, including one for RPE, one for gain, one for loss, one for reward prediction for deck A, one for reward prediction for deck B, one for reward prediction for deck C, and one for reward prediction for deck D. The value regressors were convolved with a canonical hemodynamic response function. On the first level model for RPE, for example, we set all feedback after deck selection as a regressor in the GLM design matrix. Then we conducted a parametric modulation analysis that consider corresponding RPE for each trial as another regressor in the design matrix to examine which regions encode the RPE. Then, the RPE regressor was convolved with a canonical hemodynamic response function. The RPE regressor and six noninterest regressors for head motion were simultaneously regressed against the blood oxygenation level-dependent signal in each voxel. Then, the parameter estimates were extracted for each value and for each participant. We performed a group-level one-sample t test for parameter estimates using family-wise error correction. Specifically, we used the convention that group-level results should survive at an uncorrected p value of .001, at the voxel level. Then we reported those clusters with a family-wise error corrected for multiple comparison p value of less than .05. We used the empirical, spatial autocorrelation function to estimate the smoothness and used AFNI's 3dClustSim to run a Monte Carlo simulation with 10,000 iterations in a whole-brain mask (Cox et al., 2017; Eklund et al., 2016). We performed additional group-level one-sample t test with sex as covariates for parameter estimates for value signals in the general linear model.

2.6 | Whole brain searchlight-based MVPA

We first used whole-brain searchlight-based MVPA to classify advantageous choice versus disadvantageous choice. We adapted the within-subject MVPA methods from a previous study (Zha et al., 2019). Specifically, we used the least squares-separate (LSS) method to extract choice-related activations according to a previous study (Mumford et al., 2012). LSS is the most effective method to estimate choice activation (Mumford et al., 2012) and has been widely used in the field (Corradi-Dell'Acqua et al., 2016; Piva et al., 2019; Zha et al., 2019). According to the LSS method, a general linear model was used to extract activation for each choice. The general linear model was estimated for concatenated three IGT task runs. There were 180 choices, $C_{1...180}$, including advantageous choices and disadvantageous choices, for each participant. A general linear model was run for each choice. For the ith choice, C_i, the general linear model included two choice regressors. The first was the choice regressor of interest. During a trial with choice C_i, this regressor was defined as 1 during the epoch when a button press was made in the selection phase and 0 for the other epochs; during trials with choices $C_{1...i-1,i+1...180}$, this regressor was defined as 0 for all epochs. The other was the choice regressor of nuisance. During a trial with choice C_i, this regressor was defined as 0 for all epochs; during trials with choices $C_{1...i-1,i+1...180}$, this regressor was defined as 1 during the epoch when a button press was made in the selection phase and 0 for the other epochs. The choice regressor of interest and choice regressor of nuisance were convolved with a canonical hemodynamic response function. The value of β for the choice regressor of interest in the general linear model was the activation for choice C_i. The general linear model was repeated 180 times to extract activations for 180 choices for each participant. The general linear model was performed using MATLAB's *regstats* function (MATLAB v2019a, Mathworks Inc., Natick, MA).

We implemented two steps to control the effects of values, as choices can be expected to be related to value signals, including RPE, gain, loss, and reward predictions for the four decks. For step 1, we used the Gram–Schmidt orthogonalization algorithm to orthogonalize choices and values before implementing the general linear model (Chen, 2021; Pine et al., 2009). Specifically, we orthogonalized choice and RPE, gain, loss, and reward predictions for the four decks. For step 2, the orthogonalized choice regressor of interest, the orthogonalized choice regressor of nuisance, the regressors for RPE, gain, loss, and reward predictions for the four decks (those defined as RPE, gain, loss, or reward predictions for the four decks during the epochs when feedback was presented and 0 for the other epochs), and six regressors of no interest for head motion were included in each general linear model. We extracted β, the activation of the orthogonalized choice regressor of interest, for each voxel in the whole brain in each general linear model. The extracted activations were grouped into two categories according to the choice type, that is, advantageous choice versus disadvantageous choice, for each voxel and for each participant.

We performed whole-brain searchlight-based MVPA that did not depend on a priori assumptions but searched for predictive information across the whole brain. For each voxel v_i, considering the local patterns that contained the spatial correlation that might decode advantageous choice versus disadvantageous choice, we constructed a spherical collection of voxels ($S_{1...N}$), with 33 voxels (Kriegeskorte et al., 2006) centered on voxel v_i. For each voxel ($S_{1...N}$) in the fixed spherical cluster, we extracted the parameter estimation (β value for the choice trial) separately for advantageous and disadvantageous choice trials. This generated two N-dimensional pattern vectors, namely $(\beta_{a,1...N})$ and $(\beta_{d,1...N})$, representing the local response patterns in the spherical cluster in trials in which the participants chose between advantageous options and disadvantageous options. Both $(\beta_{a,1...N})$ and $(\beta_{d,1...N})$ were normalized to the range from 0 to 1 to give all voxels equal importance during classifier training (Linn et al., 2016; Peng et al., 2013) and subsequently were used as input to a subject-wise linear support vector classification decoding analysis described below. The support vector classification was performed with a default cost parameter c = 1. The decoding accuracy of the central voxel v_i was acquired by five-fold cross-validation. The implementation of the support vector machine and cross-validation were based on *sklearn. svm.SVC* in Python's scikit-learn toolbox (version 0.21.2; Pedregosa et al., 2011). During training and testing of the classification model, random undersampling was used to handle the imbalance in samples between advantageous choice and disadvantageous choice. For example, if the number of advantageous choices was larger than that of disadvantageous choices, advantageous choices were removed randomly to make the numbers the same as the disadvantageous choices by the numpy.random.shuffle function in Python (version 3.6.8). Equal numbers of both choices were labeled the original data sample, which was then randomly partitioned into five equal sized subsamples for five-fold cross-validation. Three-voxel size spheres, that is, 123 voxels (Kriegeskorte et al., 2006), for the searchlight-based analysis was run to complement findings from the 33 voxels sphere. A leave-one-run-out cross-validation was used to complement a five-fold cross-validation procedure for the searchlight-based prediction analysis. The same procedure was performed for each voxel over the whole brain for each participant. The whole-brain decoding accuracy was normalized by subtracting the mean of the whole-brain accuracy for each participant.

We performed a group-level one-sample t test for whole-brain searchlight-based MVPA for decoding accuracy using family-wise error correction. We performed additional group-level one-sample t test with sex as covariates for decoding accuracy in the whole-brain searchlight-based MVPA.

As a control analysis, we also tested whether choice-related activations were correlated with value signals, that is, RPE, gain, loss, and reward predictions for the four decks using both whole brain analysis and region of interest (ROI) analysis. Specifically, the extracted activations in the general linear model were grouped into two categories according to the median split of the values of the trials, that is, high and low subgroups for RPE, gain, loss, and reward predictions for the four decks for each participant. We tested whether these subgroups

showed differences for RPE, reward predictions for the four decks, gain, and loss separately using paired t test in the whole brain with family-wise error correction. We further included the left and right OFC ROIs from the Anatomical Automatic Labeling atlas (AAL2; Rolls et al., 2015). The left OFC ROI included OFCmed_L, OFCant_L, OFCpost_L, and OFClat_L and the right OFC ROI included OFCmed_R, OFCant_R, OFCpost_R, and OFClat_R. The extracted activations for values above were averaged in the left and right OFC ROIs separately, then, were fed into group comparisons using the t test with Bonferroni correction to correct for multiple comparisons, as we performed seven tests for values signals.

2.7 | ROI-based MVPA

We further tested whether the OFC represented choice, that is, advantageous choices versus disadvantageous choices, using ROI-based MVPA. First, we included OFC ROIs from the AAL2 that showed overlapping areas with the peak voxel for significant clusters in the whole-brain searchlight-based MVPA. We also used the peak coordinates from the whole-brain MVPA to generate a spheric ROI with a radius of 8 mm to complement results. Second, we extracted the activations associated with each choice for each OFC ROI. Activations were also normalized to the range from 0 to 1 for advantageous choice and disadvantageous choice separately (Linn et al., 2016; Peng et al., 2013). The decoding accuracy for each OFC ROI was acquired by five-fold cross-validation.

We tested whether the decoding accuracy was greater than chance level (0.5) for each OFC ROI using a one-sample t test. We tested whether the decoding accuracy was correlated with the learning rate, total score, and total net good decks using Pearson correlations.

To test whether the signal-to-noise ratio (SNR) affected the decoding results, Pearson correlations between the SNR and decoding accuracy for each ROI were determined.

2.8 | PPI analysis

To investigate whether the functional connectivity of the OFC identified in ROI-based MVPA differed between advantageous and disadvantageous choices, we ran PPI analysis. First, we created a "seed" time series by extracting mean time courses for each OFC identified in ROI-based MVPA. Second, we computed the interaction terms between the "seed" and either the (1) advantageous choice regressor, defined as 1 during the epoch when a button press was made and 0 for other epochs during trials with advantageous choice and as 0 for all epochs during trials with disadvantageous choice or the (2) disadvantageous choice regressor, defined as 1 during the epoch when a button press was made and 0 for other epochs during trials with disadvantageous choice and as 0 for all epochs during trials with advantageous choice. Third, we estimated a PPI general linear model including the following regressors: (1) the advantageous choice

	Mean	SD	Min	Max
Learning rate	0.152	0.119	0.012	0.605
Response time	0.655	0.240	0.273	1.424
The number of advantageous choices	136.426	20.752	83.000	168.000
The number of disadvantageous choices	43.574	20.752	12.000	97.000
Total score	5050.741	977.772	3075	6885
Total net good decks	92.852	41.503	−14.000	156.000

TABLE 1 Summary of behavioral performance in the Iowa gambling task

regressor, (2) the disadvantageous choice regressor, (3) the OFC seed time course, (4) the interaction term between the "seed" and advantageous choice regressor, defined as advantageous choice PPI, (5) the interaction term between the "seed" and disadvantageous choice regressor, defined as disadvantageous choice PPI, (6) seven value regressors including RPE, gain, loss, and reward predictions for the four decks, defined as RPE, gain, loss, or reward predictions for the four decks, respectively, during the epochs when feedback was presented and 0 for the other epochs, and (7) six noninterest regressors for head motion. The advantageous choice regressor, the disadvantageous choice regressor, the interaction term between the "seed" and advantageous choice, the interaction term between the "seed" and disadvantageous choice, and seven value regressors were convolved with a canonical hemodynamic response function. The PPI general linear model was performed using AFNI's *3dDeconvolve*.

We computed the first level contrast for the disadvantageous choice PPI β minus the advantageous choice PPI β. We performed a one-sample t test to identify significant differences in the contrast to identify PPI effects using family-wise error correction.

We also tested whether there were overlapping regions in the brain among the whole-brain searchlight-based MVPA and PPI.

As a control analysis, we tested whether value signals modulated OFC functional connectivity. To achieve this, we performed PPI analysis for RPE, gain, loss, and reward predictions for the four decks separately. The PPI general linear model included the following regressors: (1) a value regressor, defined as RPE, gain, loss, or reward predictions for the four decks during the epochs when feedback was presented and 0 for other epochs, (2) the OFC seed time course, (3) the interaction term between the "seed" and value regressor, defined as the value PPI, and (4) six noninterest regressors for head motion. We computed the first level contrast for PPI β values and performed a one-sample t test to identify PPI effects using family-wise error correction. Therefore, we have run eight PPI analyses, including one advantageous choice versus disadvantageous choice, one RPE, one gain, one loss, one reward prediction for deck A, one reward prediction for deck B, one reward prediction for deck C, and one reward prediction for deck D. Thus, the PPI was prone to generate false positives. Gotts et al. (2021) have used a cluster-size correction to control the Type I error rate in fMRI task-based functional connectivity analyses (Gotts et al., 2021). Specifically, the family-wise alpha for multiple-comparisons correction was set at p <(.05/[number of tests * number of seeds]) in order to correct for a number of tests as well as a number of seeds, with the full FWE Type I error rate

controlled at p <.05. Thus, we used the same method to control the Type I error rate: A number of tests were eight; thus, family-wise alpha for multiple-comparisons correction was set at p <(.006/number of seeds).

In the FWE correction, group-level results should survive at an uncorrected p value of .001, at voxel level. Then we reported those clusters with a family-wise error corrected for multiple comparison p value of less than (.006/number of seeds). We used the empirical, spatial autocorrelation function to estimate the smoothness and used AFNI's 3dClustSim to run a Monte Carlo simulation with 10,000 iterations in a whole-brain mask (Cox et al., 2017; Eklund et al., 2016).

3 | RESULTS

3.1 | Summary of behavioral performance in the IGT

The participants' learning rate, response time, number of advantageous choices, number of disadvantageous choices, total score, and total net good decks are summarized in Table 1.

3.2 | BOLD activity in the OFC is correlated with value signals

We found significant activations in the OFC, striatum, and posterior cingulate cortex for value signals, including RPE, gain, loss (Figure 2 and Table 2), and reward predictions for the four decks (Figure S1 and Table S1). Using the general linear model for value signals with sex as covariates, we also found significant activations in the OFC, striatum, and posterior cingulate cortex for value signals, including RPE, gain, loss, and reward predictions for the four decks (Figures S2 and S3). Therefore, the results are consistent with previous studies showing that the OFC is implicated in value evaluation (Antony et al., 2021; Tom et al., 2007; Wang et al., 2017).

3.3 | The OFC represents advantageous choice

As the OFC has been implicated in the representation of value signals, we next examined whether the OFC represented advantageous

FIGURE 2 BOLD activity in the OFC was correlated with value signals. BOLD signals in the OFC, striatum, and posterior cingulate cortex were correlated with value signals, including (a) RPE, (b) gain, and (c) loss. Family-wise error at a cluster-level threshold of $p < .05$ (voxel-level threshold of $p < .001$, voxel size >13 for RPE, 33 for gain, and 19 for loss). $N = 54$
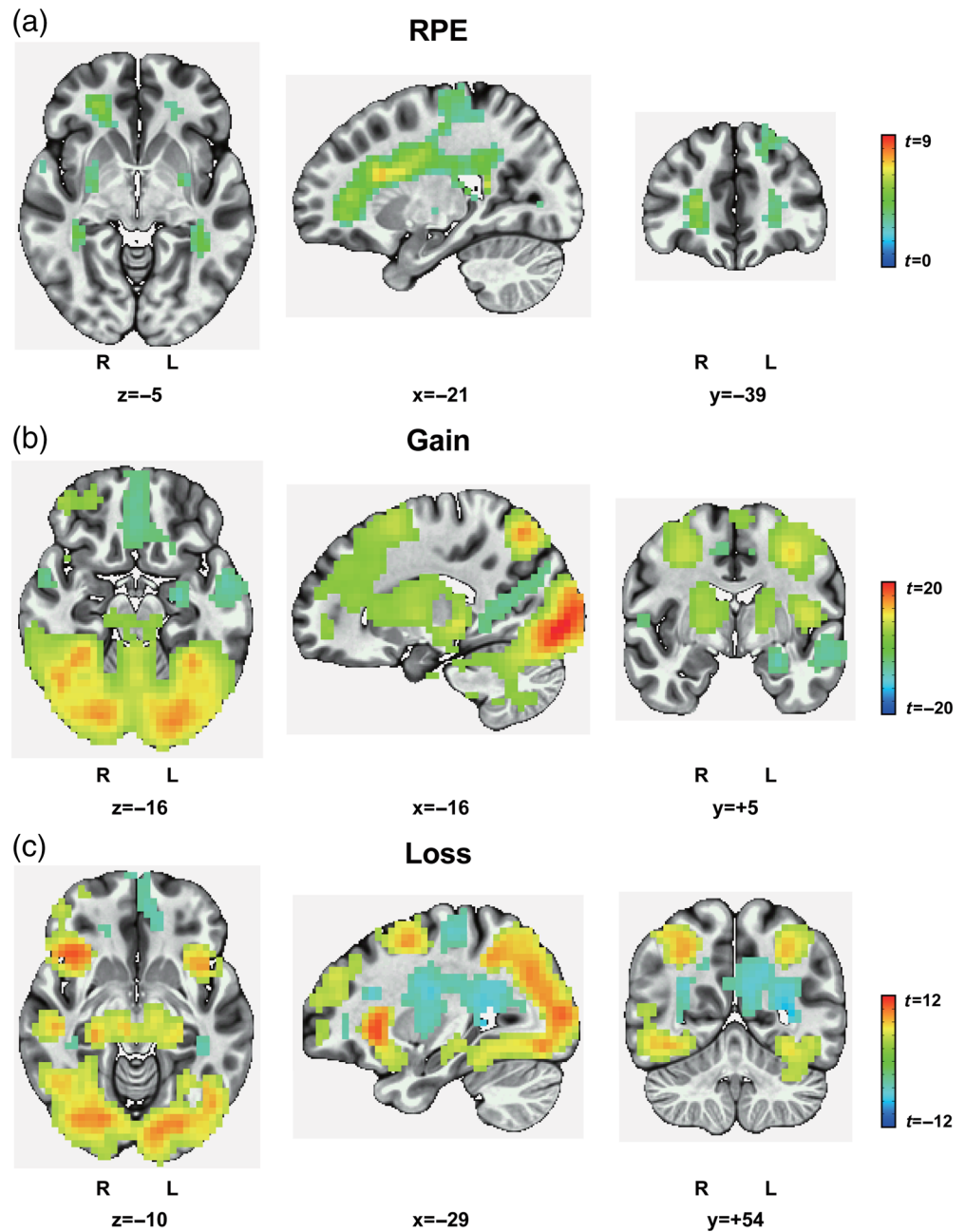
choice while controlling for value effects. Using whole-brain searchlight-based MVPA, we found that the activity pattern in the OFC indeed represented advantageous choice (Figure 3a and Table 3). A leave-one-run-out cross-validation revealed a consistent result: The activity pattern in the OFC represented advantageous choice (Figure S4a). A whole-brain searchlight-based MVPA with a three-voxel size sphere revealed a consistent result: The activity pattern in the OFC represented advantageous choice (Figure S4b). Using whole-brain searchlight-based MVPA with sex as covariates, we also found that the activity pattern in the OFC indeed represented advantageous choice (Figure S4c). Whole-brain searchlight-based MVPA also revealed that activity in the frontal regions and the parietal regions represented advantageous choice (Figure 3a and Table 3); thus, we replicated similar findings regarding the representation of

choice in the frontoparietal network from previous studies (Hunt et al., 2014; Kable & Glimcher, 2009).

Are choice related activations in the OFC related to value signals? We found that there were no significant activations in the OFC between the high and low subgroups for RPE, gain, loss (Figure 3b–d, and Table S3), or reward predictions for the four decks (Figure S5 and Table S4). We further found that there were no significant differences in the left or right OFC ROIs between the high and low subgroups for RPE, gain, and loss (all p_s >.35, corrected). The results suggest that choice-related activations in the OFC for MVPA were not confounded by value signals.

The peak voxels of significant clusters in the whole-brain searchlight-based MVPA showed an overlapping area with OFCmed_R in AAL2; therefore, we further examined the choice representation in OFCmed_R

TABLE 2   Blood oxygenation level-dependent activity in the orbitofrontal cortex is correlated with the value signals

	Brain regions	Voxels	x[a]	y	z
RPE	Right inferior frontal gyrus	2450	−26	−22	+24
	Left superior frontal gyrus	43	+22	−42	+48
	Left superior frontal gyrus	37	+18	−62	+12
	Right cerebellum	20	−42	+78	−36
	Left cerebellum	19	+10	+46	−16
Gain	Right lingual gyrus	11,827	−18	+90	−4
	Left hippocampus	337	+26	+10	−16
	Left mid orbital gyrus	301	+2	−54	−12
	Right medial temporal pole	124	−50	−14	−28
	Right Rolandic operculum	80	−42	+14	+20
	Right SMA	75	−6	+10	+52
	Right angular gyrus	42	−58	+66	+28
Loss	Right insula lobe	4508	−34	−22	+0
	Right inferior parietal lobule	3604	−42	+42	+48
	Left paracentral lobule	531	+6	+30	+64
	Left middle frontal gyrus	65	+50	−38	+20
	Right cerebellum	28	−42	+82	−36
	Left superior frontal gyrus	25	+18	−46	+48

[a]The coordinates of the peak voxel are shown in MNI space (+ left, − right; + posterior, − anterior; + superior, − inferior). Family-wise error at a cluster-level threshold of $p < 0.05$ (voxel-level threshold of $p < 0.001$, voxel size > 13 for RPE, 33 for gain, and 19 for loss). N = 54.

using ROI-based MVPA. We found that OFCmed_R represented an advantageous choice ($t_{53} = 7.770, p < .001$, Cohen's $d = 1.057$, 95% confidence interval: [0.075, 0.126]) (Figure 4a). We found significant correlations between the decoding accuracy and learning rate ($r = .559, p < .001, N = 54$), total score ($r = .357, p = .008, N = 54$), and total net good decks ($r = .468, p < .001, N = 54$; Figure 4b–d). The decoding accuracy showed no significant correlations with the SNR ($r = −.119, p = .390, N = 54$) or censor rate ($r = .071, p = .610, N = 54$), suggesting that the decoding accuracy was not explained by either of these parameters. The peak coordinate from the whole-brain MVPA, that is, ($−14, −38, −20$), was used to generate a spheric ROI with radius 8 mm. The ROI-based MVPA using this spheric ROI revealed a consistent result: The activity pattern in the OFC represented advantageous choice ($t_{53} = 2.062, p < .041$, Cohen's $d = 0.281$, 95% confidence interval: [4.440e − 04, 0.032]).

3.4 | Choice modulates OFC functional connectivity with the superior medial gyrus

PPI analysis revealed greater OFC connectivity with the superior medial gyrus when choosing disadvantageous options versus choosing advantageous options (Figure 5a). Furthermore, the superior medial gyrus showed an overlapping area with brain regions representing advantageous choice revealed by whole-brain searchlight-based MVPA (Figure 5b). As a control analysis, we tested whether value signals modulated OFC functional connectivity. We found that there

was no significant OFC functional connectivity in the whole brain for RPE, gain, loss, or reward predictions for the four decks (Figure 5c), suggesting that choice-modulated OFC functional connectivity was not confounded by the value signals.

4 | DISCUSSION

Consistent with the proposal of a good-based model, the present study demonstrates that the OFC represents advantageous choice, which provides strong evidence to support the role of the OFC in binary choice in the IGT. Furthermore, IGT behavioral performances were correlated with the advantageous choice representation in the OFC. Third, the functional connectivity between the OFC and superior medial gyrus supports choice.

4.1 | The OFC represents an advantageous choice in the IGT

In the present study, we demonstrated that the OFC represents binary choice in the IGT based on the distributed activity pattern. These results are supported by neurobiological studies with human (Bechara et al., 1997; Manes et al., 2002) as well as animal (Bradfield et al., 2015; Stolyarova & Izquierdo, 2017) prefrontal lesions (including in the OFC), consistently indicating that the OFC plays a necessary role in decision-making when information is complex.

(a) **The OFC represents advantageous choice**

(b) **Choice related activations in the OFC are not correlated with RPE**

(C) **Choice related activations in the OFC are not correlated with gain**

(D) **Choice related activations in the OFC are not correlated with loss**

R   L
z=−20

x=−14

R   L
y=−38
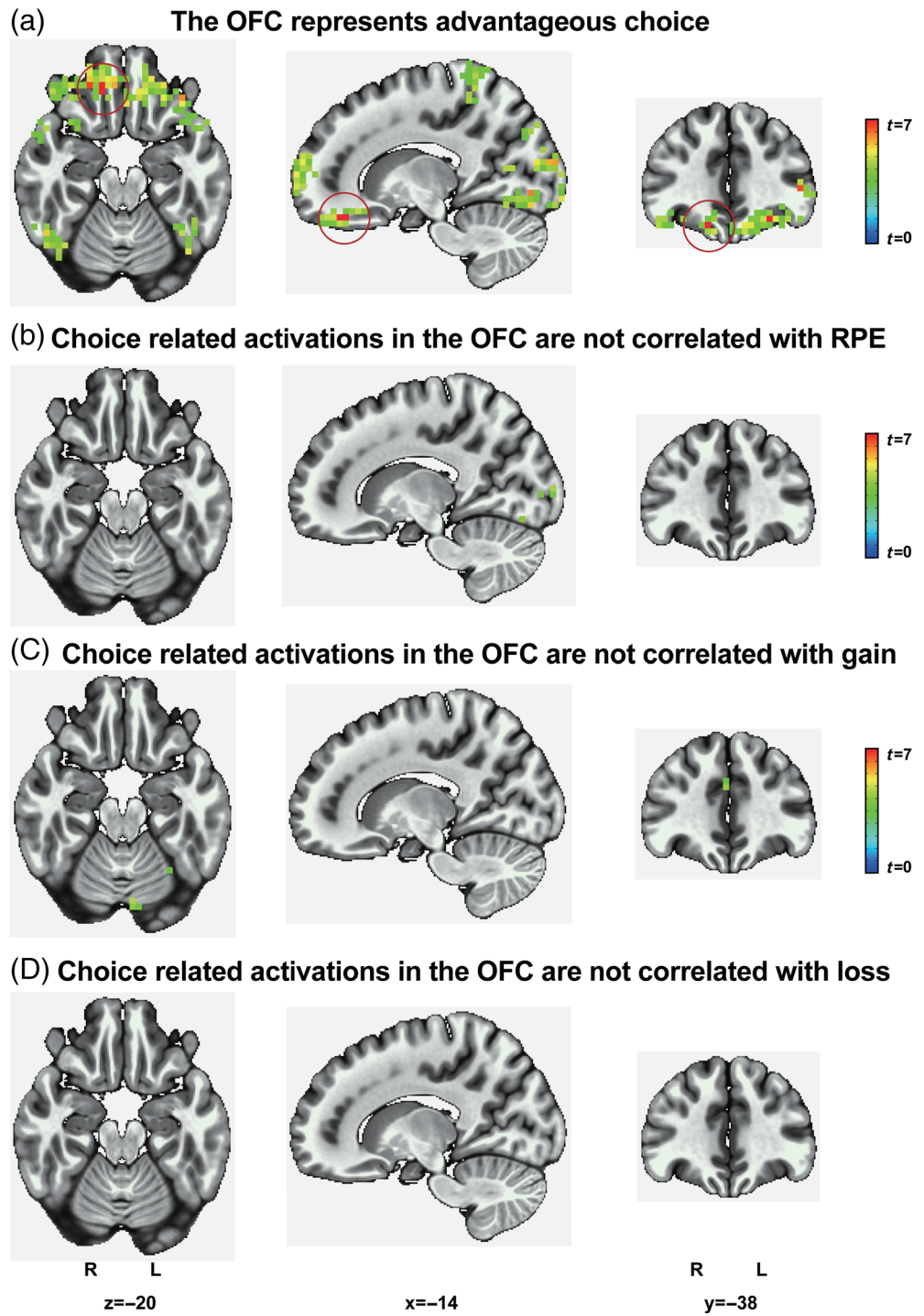
Abnormal behavioral performance in the IGT has been implicated in several brain disorders. For example, Linhartová et al. (2020) have shown that attention-deficit/hyperactivity disorder shows significant impairment in the IGT compared to healthy controls (Linhartová et al., 2020). Yang et al. (2019) have shown decreased win and loss feedback-elicited activations in the OFC in the attention-deficit/hyperactivity disorder compared to healthy controls (Yang et al., 2019). Using a univariate analysis, Norman et al. (2018) did not show altered advantageous choice-elicited activations in the OFC attention-deficit/hyperactivity disorder compared to healthy controls

(Norman et al., 2018). For cigarette smoking, Wei et al. (2018) have shown that smokers have a low learning rate in the IGT compared to healthy controls (Wei et al., 2018). Moreover, Wei et al. (2018) have shown that the medial prefrontal cortex did not modulate RPE learning in smokers compared to healthy controls (Wei et al., 2018). Consistent with the idea that the OFC represents a cytoarchitectonic and functionally heterogeneous region (Rolls, 2021; Wallis, 2011), our MVPA results may suggest that the multivariate activity pattern in the OFC may be altered in the IGT advantageous choice for attention-deficit/hyperactivity disorder and smokers.

TABLE 3 Brain regions including the orbitofrontal cortex that represent advantageous choice

Brain regions	Voxels	x[a]	y	z
Right inferior occipital gyrus	497	−38	+82	−16
Right superior medial gyrus	157	−10	−66	+20
Left superior orbital gyrus	135	+14	−62	−8
Right superior orbital gyrus	130	−14	−38	−20
Left superior temporal gyrus	72	+54	+38	+20
Right middle temporal gyrus	59	−54	+38	+4
Left insula lobe	46	+42	−6	−12
Right paracentral lobule	45	−2	+38	+76
Right superior occipital gyrus	42	−30	+78	+40
Left inferior occipital gyrus	39	+46	+74	−8
Right temporal pole	36	−62	−2	+0
Right temporal pole	28	−54	−14	−16
Right angular gyrus	27	−50	+70	+36
Left superior parietal lobule	27	+22	+46	+64
Left superior parietal lobule	26	+30	+66	+64
Left inferior occipital gyrus	22	+18	+98	−8
Left temporal pole	20	+58	−10	−4
Left postcentral gyrus	20	+66	+14	+16

[a]The coordinates of the peak voxel are shown in MNI space (+ left, − right; + posterior, − anterior; + superior, − inferior). Family-wise error at a cluster-level threshold of $p < 0.05$ (voxel-level threshold of $p < 0.001$, voxel size > 4). This table only displays the brain regions that formed a cluster of more than 20 voxels; all significant clusters are shown in Supplementary Table 2. $N = 54$.

In the present study, significant clusters in the whole-brain searchlight-based MVPA mainly included the medial part of the OFC (see Section 3.3 and Figure 3a). Studies have shown a subjective value role in the medial OFC (Clithero & Rangel, 2014; Levy & Glimcher, 2012). Our findings suggest that the medial OFC can also represent a choice role. The finding that both the overall value and binary choice were represented in the medial OFC may suggest that the medial OFC can compute the value and then form a choice in an efficient way. There are many forms of economic decision-making. Whether the choice role in the medial OFC could be generalized to other forms of economic decision-making should be tested in future work.

Furthermore, beyond the OFC, the frontoparietal network was also implicated in choice in the present study, and the finding is consistent with previous studies (Hunt et al., 2014; Kable & Glimcher, 2009). Both the OFC and the frontoparietal network represented choice in the present study; therefore, we expected to find functional connectivity between the regions for choice. Indeed, we identified a functional connectivity between the OFC and the superior medial gyrus for choice, but not for values, suggesting that the OFC is functionally coupled with the prefrontal cortex when humans make choices. As the frontoparietal network has been widely implicated various decision-making situations

(Hunt et al., 2014; Kable & Glimcher, 2009), the connectivity between the OFC and the superior medial gyrus would be helpful for choice under various decision-making contexts. We also found that OFC activity is related to value signals, for example, RPE, gain, and loss. Therefore, the finding that both choice and value were represented in the OFC may make it easier for individuals to make optimal choices with the help of frontoparietal network modulation during difficult decision-making situations that lack sufficient information.

Patients with insula lesion have shown poor IGT performance (Bechara, 2004). Disadvantageous choice versus advantageous choice activated the insula (Brevers et al., 2016; Lawrence et al., 2009). Patients with temporal lobe resection, including temporal pole, show impairments in the IGT performance compared to healthy controls (Von Siebenthal et al., 2017). The middle temporal cortex has been shown higher activation during disadvantageous choice versus advantageous choice (Ma et al., 2015). Together, our finding that activity pattern in the insula, as well as the temporal pole, represented an advantageous choice in the IGT suggests an important role of the insula and temporal pole in decision-making.

4.2 | A proposed role for the OFC: representation of choice-related complex information along a continuous spectrum

In the present study, the OFC was shown to represent advantageous choice. This finding is supported by a recently proposed cognitive map representing a state space (Wilson et al., 2014). In the context of the cognitive map, the OFC is activated when the decision maker becomes cognizant of unobservable information and makes a correct choice; however, the OFC would not activate when the decision maker is not cognizant of unobservable information and makes an incorrect choice (Schuck et al., 2016).

Interestingly, in the present study, even though the participants did not know the specific reward value for each deck, the OFC nevertheless represented advantageous choice. Integration of these findings shows that exact knowledge of complex information is not necessary for OFC activation. This may suggest that the OFC, in part, could play a role in unconscious influences, for example, emotions, in complex decision-making (Poppa & Bechara, 2018).

We found that decoding accuracy in the OFC correlated with decision-making performance. We therefore propose a role for the human OFC based on the cognitive map idea: the OFC may represent choice-related complex information along a continuum, for example, from a high decoding accuracy of advantageous choice if the decision maker exactly knows the complex information to a low decoding accuracy if they do not. Our proposal further predicts that the OFC represents choice in choosing between other decision-making parameters, such as self-control and cost. This is important because humans often face choices that have unknown costs for effort control. It is beneficial to exert an appropriate level of effort for an appropriate choice. The OFC seems to be a candidate for the brain region
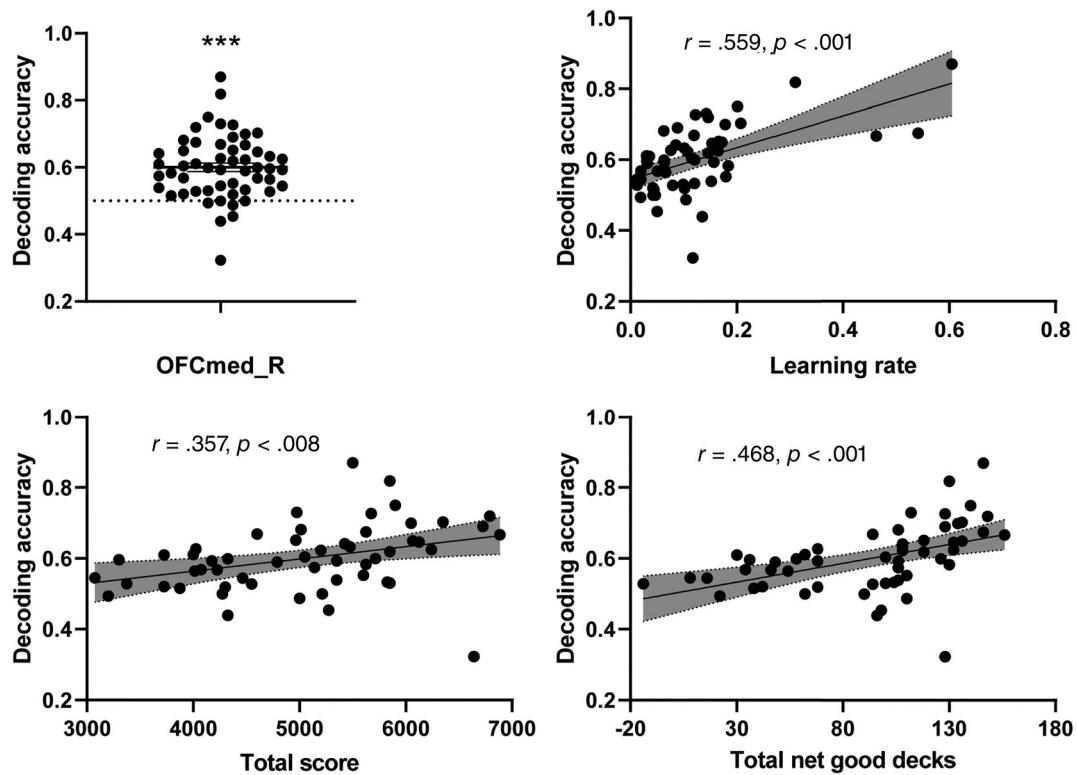
FIGURE 4 The OFC represents an advantageous choice, and the OFC decoding accuracy is correlated with behavioral performances. (a) The OFCmed_R region in AAL2 represents an advantageous choice. The OFCmed_R decoding accuracy was correlated with the (b) learning rate, (c) total score, and (d) total net good decks in the IGT. The dashed line in the panels shows the chance level (0.5), and the dashed area in the panels shows the 95% confidence interval. $N = 54$

used when making choices based on the aforementioned parameters in a complex context; this hypothesis should be investigated in future work.

In the present study, as shown in Figure 2, there was a big engagement of the occipito-temporal cortex in the IGT. This is consistent with findings in a previous study (Wang et al., 2017). Specifically, Wang et al. (2017) have shown that the significant clusters for the RPE as well as the reward predictions are very large. That big engagement of the occipito-temporal cortex is implicated in RPE and reward predictions in the IGT. A potential reason for clusters being large in Wang et al. (2017) as well as in the present study is that a less stringent voxel-level threshold was used in the FWE correction in both studies. For example, we used p <.001 and Wang et al. (2017) used p <.005.

Moreover, in the present study, we found that beyond striatum and OFC, the occipito-temporal cortex was also activated for RPE in the IGT. Previous studies have also shown a nonspecific cluster in the IGT task during fMRI. Specifically, Wei et al. (2018) have shown that numerous brain regions were involved in the significant clusters for the RPE including the occipito-temporal cortex. Tanabe et al. (2013) have also shown that activations in the temporal and occipital cortex have been involved in RPE in the IGT. A potential reason for nonspecific cluster in Wei et al. (2018), Tanabe et al. (2013), and the present study may be that the IGT is a complex task involving gain, loss, and learning than a normal task with RPE, such as decision-making

involving risk. For example, Wang et al. (2017) have found that the RPE activated more brain regions in the IGT than in the risky decision-making task. More future work is needed to test this possibility.

Several shortcomings of the present study should be acknowledged. First, few female participants were recruited in the present study. We conducted ROI-based MVPA for males and females separately to test whether females and males showed a difference in decoding accuracy. We found consistent results (see Table S5) between the sexes, suggesting that the percentage of females might not influence our results. Future work should include more female participants to substantiate our conclusion. Second, the IGT design convolves decision-making with uncertainty with learning. Good learning would presumably result in choosing from the high value deck and not from the other decks and would also presumably result in choosing from the high value deck more in the late IGT runs and less in the early IGT runs. Therefore, a reasonable assumption would be that changes in activation patterns between choosing high value versus choosing low value may be due to differences in choice probability. However, the choice probability is related to reward prediction, which we controlled for when we performed MVPA and PPI analysis. We found that choice-related activations in the OFC could represent choice in MVPA and that choice-related activations in the OFC were not related to reward predictions. We also found that choice, but not reward predictions, modulated OFC functional connectivity with the superior medial gyrus in PPI analysis. Therefore,
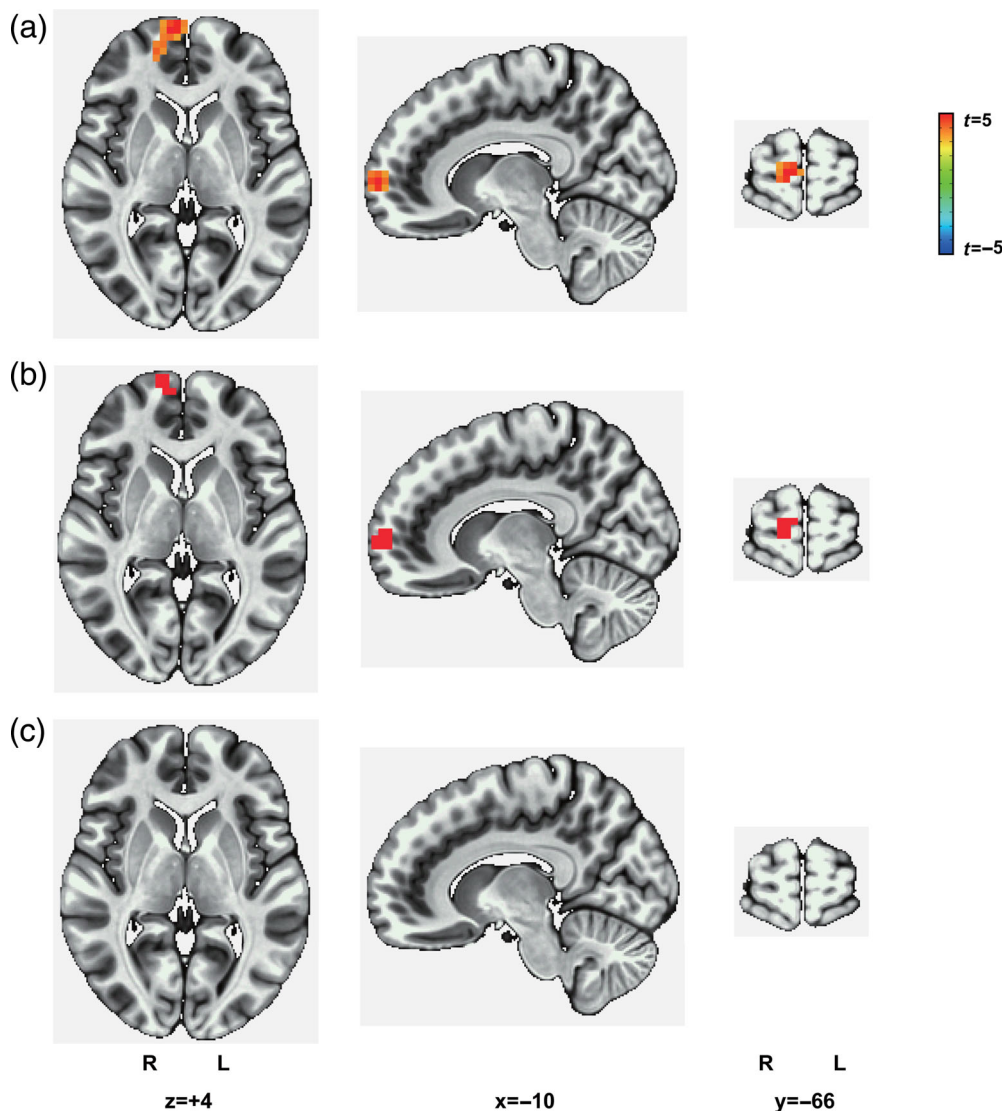
FIGURE 5 The OFC is functionally connected with the superior medial gyrus for choice, but not for values. (a) Compared with advantageous choice, disadvantageous choice increased the OFC functional connectivity with the superior medial gyrus. Voxel size: 40; peak voxel coordinates: −10, −66, +4. R, right, L, left. Family-wise error at a cluster-level threshold of p <.006 (voxel-level threshold of p <.001, minimum cluster size k = 32 voxels). (b) The overlapping area between the superior medial gyrus and the brain regions representing advantageous choice contained 16 voxels. (c) There was no significant OFC functional connectivity across the whole brain for RPE, gain, loss, or reward predictions for the four decks. Family-wise error at a cluster-level threshold of p <.006 (voxel-level threshold p <.001, minimum cluster size k = 33 for gain, 57 for loss, 30 for RPE, 38 for reward prediction for deck A, 43 for reward prediction for deck B, 34 for reward prediction for deck C, and 40 for reward prediction for deck D). N = 54

our results suggest that neither the choice probability nor the learning effect in the IGT confounds the decoding or PPI results in the present study. Future work will require a complex decision-making task without learning to substantiate our conclusion. Third, attention modulates the value signal in the OFC (Xie et al., 2018), thus, a reasonable assumption would be that choice-related signals in the OFC may be confounded with attention. However, the OFC signal has been related to value of attended option (Xie et al., 2018) and we found that choice-related signals in the OFC were not related to all value signals, including RPE, gain, loss, or reward predictions for four decks. Therefore, our results suggest that attention may not confound the decoding or PPI results in the present study. Future work will require a decision-making task with covert shift of attention to substantiate our conclusion. Fourth, the deck A and B were presented in the left-hand side, and the deck C and D were presented in the right-hand side of the computer display. Thus, the choice-related signals cannot be dissociated from spatial information within each participant. However, findings that decoding accuracy in the OFC were related to the behavioral performance in IGT,

suggesting that spatial information might not confound decoding accuracy of choice in the present study.

5 | CONCLUSION

In conclusion, our results demonstrate that the OFC represents advantageous choice in the IGT. Our data provide evidence to support the integration of knowledge in the OFC to make choices in a complex context, which may be helpful for survival. Decreased decoding accuracy in the OFC may be related to poor decision-making ability, and these findings may provide potential insight into understanding impulsive behaviors.

CONFLICT OF INTEREST

The authors declare no potential conflict of interest.

AUTHOR CONTRIBUTIONS

Rujing Zha: conceptualization, formal analysis, methodology, software, data curation, writing-original draft preparation, project administration; **Peng Li:** data curation, formal analysis, methodology, writing-reviewing and editing; **Ying Liu:** methodology; **Abdulqawi Alarefi:** writing-reviewing; **Xiaochu Zhang:** supervision, conceptualization, methodology, writing-reviewing and editing; **Jun Li:** supervision, conceptualization, methodology, writing-reviewing and editing.

DATA AVAILABILITY STATEMENT

All data were available from the authors.

ORCID

Rujing Zha https://orcid.org/0000-0003-0457-096X
Xiaochu Zhang https://orcid.org/0000-0002-7541-0130

REFERENCES

Antony, J. W., Hartshorne, T. H., Pomeroy, K., Gureckis, T. M., Hasson, U., McDougle, S. D., & Norman, K. A. (2021). Behavioral, physiological, and neural signatures of surprise during naturalistic sports viewing. *Neuron*, *109*(2), 377–390. https://doi.org/10.1016/j.neuron.2020.10.029

Ballesta, S., Shi, W., Conen, K. E., & Padoa-Schioppa, C. (2020). Values encoded in orbitofrontal cortex are causally related to economic choices. *Nature*, *588*(7838), 450–453. https://doi.org/10.1038/s41586-020-2880-x

Bartra, O., McGuire, J. T., & Kable, J. W. (2013). The valuation system: A coordinate-based meta-analysis of BOLD fMRI experiments examining neural correlates of subjective value. *NeuroImage*, *76*, 412–427. https://doi.org/10.1016/j.neuroimage.2013.02.063

Bechara, A. (2004). Disturbances of emotion regulation after focal brain lesions. *International Review of Neurobiology*, *62*, 159–193. https://doi.org/10.1016/s0074-7742(04)62006-x

Bechara, A., Damasio, H., Tranel, D., & Damasio, A. R. (1997). Deciding advantageously before knowing the advantageous strategy. *Science*, *275*(5304), 1293–1295. https://doi.org/10.1126/science.275.5304.1293

Behrens, T. E., Woolrich, M. W., Walton, M. E., & Rushworth, M. F. (2007). Learning the value of information in an uncertain world. *Nature Neuroscience*, *10*(9), 1214–1221. https://doi.org/10.1038/nn1954

Betz, L. T., Brambilla, P., Ilankovic, A., Premkumar, P., Kim, M. S., Raffard, S., Bayard, S., Hori, H., Lee, K. U., Lee, S. J., Koutsouleris, N., & Kambeitz, J. (2019). Deciphering reward-based decision-making in schizophrenia: A meta-analysis and behavioral modeling of the Iowa gambling task. *Schizophrenia Research*, *204*, 7–15. https://doi.org/10.1016/j.schres.2018.09.009

Bradfield, L. A., Dezfouli, A., van Holstein, M., Chieng, B., & Balleine, B. W. (2015). Medial orbitofrontal cortex mediates outcome retrieval in partially observable task situations. *Neuron*, *88*(6), 1268–1280. https://doi.org/10.1016/j.neuron.2015.10.044

Brevers, D., Noël, X., He, Q., Melrose, J. A., & Bechara, A. (2016). Increased ventral-striatal activity during monetary decision making is a marker of problem poker gambling severity. *Addiction Biology*, *21*(3), 688–699. https://doi.org/10.1111/adb.12239

Burke, C. J., & Tobler, P. N. (2011). Coding of reward probability and risk by single neurons in animals. *Frontiers in Neuroscience*, *5*, 121. https://doi.org/10.3389/fnins.2011.00121

Cai, X., & Padoa-Schioppa, C. (2019). Neuronal evidence for good-based economic decisions under variable action costs. *Nature Communications*, *10*(1), 393. https://doi.org/10.1038/s41467-018-08209-3

Chen, M. (2021). Gram-Schmidt orthogonalization. https://www.mathworks.com/matlabcentral/fileexchange/55881-gram-schmidt-orthogonalization

Chen, Z., Guo, Y., Zhang, S., & Feng, T. (2019). Pattern classification differentiates decision of intertemporal choices using multi-voxel pattern analysis. *Cortex*, *111*, 183–195. https://doi.org/10.1016/j.cortex.2018.11.001

Christakou, A., Brammer, M., Giampietro, V., & Rubia, K. (2009). Right ventromedial and dorsolateral prefrontal cortices mediate adaptive decisions under ambiguity by integrating choice utility and outcome evaluation. *The Journal of Neuroscience*, *29*(35), 11020–11028. https://doi.org/10.1523/JNEUROSCI.1279-09.2009

Clithero, J. A., & Rangel, A. (2014). Informatic parcellation of the network involved in the computation of subjective value. *Social Cognitive and Affective Neuroscience*, *9*(9), 1289–1302. https://doi.org/10.1093/scan/nst106

Corradi-Dell'Acqua, C., Tusche, A., Vuilleumier, P., & Singer, T. (2016). Cross-modal representations of first-hand and vicarious pain, disgust and fairness in insular and cingulate cortex. *Nature Communications*, *7*, 10904. https://doi.org/10.1038/ncomms10904

Cox, R. W. (1996). AFNI: Software for analysis and visualization of functional magnetic resonance neuroimages. *Computers and Biomedical Research*, *29*(3), 162–173. https://doi.org/10.1006/cbmr.1996.0014

Cox, R. W., Chen, G., Glen, D. R., Reynolds, R. C., & Taylor, P. A. (2017). FMRI clustering in AFNI: False-positive rates redux. *Brain Connectivity*, *7*(3), 152–171. https://doi.org/10.1089/brain.2016.0475

Ding, Y., Pereira, F., Hoehne, A., Beaulieu, M. M., Lepage, M., Turecki, G., & Jollant, F. (2017). Altered brain processing of decision-making in healthy first-degree biological relatives of suicide completers. *Molecular Psychiatry*, *22*(8), 1149–1154. https://doi.org/10.1038/mp.2016.221

Du, J., Rolls, E. T., Cheng, W., Li, Y., Gong, W., Qiu, J., & Feng, J. (2020). Functional connectivity of the orbitofrontal cortex, anterior cingulate cortex, and inferior frontal gyrus in humans. *Cortex*, *123*, 185–199. https://doi.org/10.1016/j.cortex.2019.10.012

Eklund, A., Nichols, T. E., & Knutsson, H. (2016). Cluster failure: Why fMRI inferences for spatial extent have inflated false-positive rates. *Proceedings of the National Academy of Sciences of the United States of America*, *113*(28), 7900–7905. https://doi.org/10.1073/pnas.1602413113

Esteban, O., Markiewicz, C. J., Blair, R. W., Moodie, C. A., Isik, A. I., Erramuzpe, A., Kent, J. D., Goncalves, M., DuPre, E., Snyder, M., Oya, H., Ghosh, S. S., Wright, J., Durnez, J., Poldrack, R. A., & Gorgolewski, K. J. (2019). fMRIPrep: A robust preprocessing pipeline for functional MRI. *Nature Methods*, *16*(1), 111–116. https://doi.org/10.1038/s41592-018-0235-4

Faul, F., Erdfelder, E., Lang, A. G., & Buchner, A. (2007). G*Power 3: A flexible statistical power analysis program for the social, behavioral, and

biomedical sciences. *Behavior Research Methods*, *39*(2), 175–191. https://doi.org/10.3758/bf03193146

Fukui, H., Murai, T., Fukuyama, H., Hayashi, T., & Hanakawa, T. (2005). Functional activity related to risk anticipation during performance of the Iowa gambling task. *NeuroImage*, *24*(1), 253–259. https://doi.org/10.1016/j.neuroimage.2004.08.028

Gotts, S. J., Milleville, S. C., & Martin, A. (2021). Enhanced inter-regional coupling of neural responses and repetition suppression provide separate contributions to long-term behavioral priming. *Communications Biology*, *4*(1), 487. https://doi.org/10.1038/s42003-021-02002-7

Hare, T. A., Camerer, C. F., & Rangel, A. (2009). Self-control in decision-making involves modulation of the vmPFC valuation system. *Science*, *324*(5927), 646–648. https://doi.org/10.1126/science.1168450

Heather Hsu, C. C., Rolls, E. T., Huang, C. C., Chong, S. T., Zac Lo, C. Y., Feng, J., & Lin, C. P. (2020). Connections of the human orbitofrontal cortex and inferior frontal gyrus. *Cerebral Cortex*, *30*(11), 5830–5843. https://doi.org/10.1093/cercor/bhaa160

Hsu, M., Bhatt, M., Adolphs, R., Tranel, D., & Camerer, C. F. (2005). Neural systems responding to degrees of uncertainty in human decision-making. *Science*, *310*(5754), 1680–1683. https://doi.org/10.1126/science.1115327

Hunt, L. T., Dolan, R. J., & Rehrens, T. E. J. (2014). Hierarchical competitions subserving multi-attribute choice. *Nature Neuroscience*, *17*(11), 1613–1622. https://doi.org/10.1038/nn.3836

Jollant, F., Lawrence, N. S., Olie, E., O'Daly, O., Malafosse, A., Courtet, P., & Phillips, M. L. (2010). Decreased activation of lateral orbitofrontal cortex during risky choices under uncertainty is associated with disadvantageous decision-making and suicidal behavior. *NeuroImage*, *51*(3), 1275–1281. https://doi.org/10.1016/j.neuroimage.2010.03.027

Kable, J. W., & Glimcher, P. W. (2007). The neural correlates of subjective value during intertemporal choice. *Nature Neuroscience*, *10*(12), 1625–1633. https://doi.org/10.1038/nn2007

Kable, J. W., & Glimcher, P. W. (2009). The neurobiology of decision: Consensus and controversy. *Neuron*, *63*(6), 733–745. https://doi.org/10.1016/j.neuron.2009.09.003

Kahnt, T. (2018). A decade of decoding reward-related fMRI signals and where we go from here. *NeuroImage*, *180*(Pt A), 324–333. https://doi.org/10.1016/j.neuroimage.2017.03.067

Kahnt, T., Weber, S. C., Haker, H., Robbins, T. W., & Tobler, P. N. (2015). Dopamine D2-receptor blockade enhances decoding of prefrontal signals in humans. *The Journal of Neuroscience*, *35*(9), 4104–4111. https://doi.org/10.1523/JNEUROSCI.4182-14.2015

Kennerley, S. W., Dahmubed, A. F., Lara, A. H., & Wallis, J. D. (2009). Neurons in the frontal lobe encode the value of multiple decision variables. *Journal of Cognitive Neuroscience*, *21*(6), 1162–1178. https://doi.org/10.1162/jocn.2009.21100

Kirwan, C. B., Shrager, Y., & Squire, L. R. (2009). Medial temporal lobe activity can distinguish between old and new stimuli independently of overt behavioral choice. *Proceedings of the National Academy of Sciences of the United States of America*, *106*(34), 14617–14621. https://doi.org/10.1073/pnas.0907624106

Kluwe-Schiavon, B., Viola, T. W., Sanvicente-Vieira, B., Lumertz, F. S., Salum, G. A., Grassi-Oliveira, R., & Quednow, B. B. (2020). Substance related disorders are associated with impaired valuation of delayed gratification and feedback processing: A multilevel meta-analysis and meta-regression (Review). *Neuroscience and Biobehavioral Reviews*, *108*, 295–307. https://doi.org/10.1016/j.neubiorev.2019.11.016

Kriegeskorte, N., Goebel, R., & Bandettini, P. (2006). Information-based functional brain mapping. *Proceedings of the National Academy of Sciences of the United States of America*, *103*(10), 3863–3868. https://doi.org/10.1073/pnas.0600244103

Lawrence, N. S., Jollant, F., O'Daly, O., Zelaya, F., & Phillips, M. L. (2009). Distinct roles of prefrontal cortical subregions in the Iowa gambling task. *Cerebral Cortex*, *19*(5), 1134–1143. https://doi.org/10.1093/cercor/bhn154

Levy, D. J., & Glimcher, P. W. (2012). The root of all value: A neural common currency for choice. *Current Opinion in Neurobiology*, *22*(6), 1027–1038. https://doi.org/10.1016/j.conb.2012.06.001

Levy, I., Snell, J., Nelson, A. J., Rustichini, A., & Glimcher, P. W. (2010). Neural representation of subjective value under risk and ambiguity. *Journal of Neurophysiology*, *103*(2), 1036–1047. https://doi.org/10.1152/jn.00853.2009

Lin, C. H., Chiu, Y. C., Cheng, C. M., & Hsieh, J. C. (2008). Brain maps of Iowa gambling task. *BMC Neuroscience*, *9*, 72. https://doi.org/10.1186/1471-2202-9-72

Linhartová, P., Látalová, A., Barteček, R., Širůček, J., Theiner, P., Ejova, A., Hlavatá, P., Kóša, B., Jeřábková, B., Bareš, M., & Kašpárek, T. (2020). Impulsivity in patients with borderline personality disorder: A comprehensive profile compared with healthy people and patients with ADHD. *Psychological Medicine*, *50*(11), 1829–1838. https://doi.org/10.1017/s0033291719001892

Linn, K. A., Gaonkar, B., Satterthwaite, T. D., Doshi, J., Davatzikos, C., & Shinohara, R. T. (2016). Control-group feature normalization for multivariate pattern analysis of structural MRI data using the support vector machine. *NeuroImage*, *132*, 157–166. https://doi.org/10.1016/j.neuroimage.2016.02.044

Lopez-Persem, A., Bastin, J., Petton, M., Abitbol, R., Lehongre, K., Adam, C., Navarro, V., Rheims, S., Kahane, P., Domenech, P., & Pessiglione, M. (2020). Four core properties of the human brain valuation system demonstrated in intracranial signals. *Nature Neuroscience*, *23*(5), 664–675. https://doi.org/10.1038/s41593-020-0615-9

Ma, S., Zang, Y., Cheung, V., & Chan, C. C. (2015). Importance of punishment frequency in the Iowa gambling task: An fMRI study. *Brain Imaging and Behavior*, *9*(4), 899–909. https://doi.org/10.1007/s11682-015-9353-0

Malvaez, M., Shieh, C., Murphy, M. D., Greenfield, V. Y., & Wassum, K. M. (2019). Distinct cortical-amygdala projections drive reward value encoding and retrieval. *Nature Neuroscience*, *22*(5), 762–769. https://doi.org/10.1038/s41593-019-0374-7

Manes, F., Sahakian, B., Clark, L., Rogers, R., Antoun, N., Aitken, M., & Robbins, T. (2002). Decision-making processes following damage to the prefrontal cortex. *Brain*, *125*(Pt 3), 624–639. https://doi.org/10.1093/brain/awf049

McCormick, E. M., & Telzer, E. H. (2017). Adaptive adolescent flexibility: Neurodevelopment of decision-making and learning in a risky context. *Journal of Cognitive Neuroscience*, *29*(3), 413–423. https://doi.org/10.1162/jocn_a_01061

Morrison, S. E., & Salzman, C. D. (2011). Representations of appetitive and aversive information in the primate orbitofrontal cortex. *Annals of the New York Academy of Sciences*, *1239*, 59–70. https://doi.org/10.1111/j.1749-6632.2011.06255.x

Mumford, J. A., Turner, B. O., Ashby, F. G., & Poldrack, R. A. (2012). Deconvolving BOLD activation in event-related designs for multivoxel pattern classification analyses. *NeuroImage*, *59*(3), 2636–2643. https://doi.org/10.1016/j.neuroimage.2011.08.076

Nisticò, V., De Angelis, A., Erro, R., Demartini, B., & Ricciardi, L. (2021). Obsessive-compulsive disorder and decision making under ambiguity: A systematic review with meta-analysis. *Brain Sciences*, *11*(2), 143. https://doi.org/10.3390/brainsci11020143

Norman, L. J., Carlisi, C. O., Christakou, A., Murphy, C. M., Chantiluke, K., Giampietro, V., Simmons, A., Brammer, M., Mataix-Cols, D., & Rubia, K. (2018). Frontostriatal dysfunction during decision making in attention-deficit/hyperactivity disorder and obsessive-compulsive disorder. *Biological Psychiatry: Cognitive Neuroscience and Neuroimaging*, *3*(8), 694–703. https://doi.org/10.1016/j.bpsc.2018.03.009

Orsini, C. A., Trotta, R. T., Bizon, J. L., & Setlow, B. (2015). Dissociable roles for the basolateral amygdala and orbitofrontal cortex in decision-

making under risk of punishment. *The Journal of Neuroscience*, 35(4), 1368–1379. https://doi.org/10.1523/JNEUROSCI.3586-14.2015

Padoa-Schioppa, C. (2011). Neurobiology of economic choice: A good-based model. *Annual Review of Neuroscience*, 34, 333–359. https://doi.org/10.1146/annurev-neuro-061010-113648

Padoa-Schioppa, C., & Assad, J. A. (2006). Neurons in the orbitofrontal cortex encode economic value. *Nature*, 441(7090), 223–226. https://doi.org/10.1038/nature04676

Payzan-LeNestour, E., Dunne, S., Bossaerts, P., & O'Doherty, J. P. (2013). The neural representation of unexpected uncertainty during value-based decision making. *Neuron*, 79(1), 191–201. https://doi.org/10.1016/j.neuron.2013.04.037

Pedregosa, F., Varoquaux, G., Gramfort, A., Michel, V., Thirion, B., Grisel, O., Blondel, M., Prettenhofer, P., Weiss, R., Dubourg, V., Vanderplas, J., Passos, A., Cournapeau, D., Brucher, M., Perrot, M., & Duchesnay, E. (2011). Scikit-learn: Machine learning in python. *Journal of Machine Learning Research*, 12(85), 2825–2830.

Peng, X., Lin, P., Zhang, T., & Wang, J. (2013). Extreme learning machine-based classification of ADHD using brain structural MRI data. *PLoS One*, 8(11), e79476. https://doi.org/10.1371/journal.pone.0079476

Pine, A., Seymour, B., Roiser, J. P., Bossaerts, P., Friston, K. J., Curran, H. V., & Dolan, R. J. (2009). Encoding of marginal utility across time in the human brain. *The Journal of Neuroscience*, 29(30), 9575–9581. https://doi.org/10.1523/JNEUROSCI.1126-09.2009

Piva, M., Velnoskey, K., Jia, R., Nair, A., Levy, I., & Chang, S. W. (2019). The dorsomedial prefrontal cortex computes task-invariant relative subjective value for self and other. *eLife*, 8, e44939. https://doi.org/10.7554/eLife.44939

Poppa, T., & Bechara, A. (2018). The somatic marker hypothesis: Revisiting the role of the 'body-loop' in decision-making. *Current Opinion in Behavioral Sciences*, 19, 61–66. https://doi.org/10.1016/j.cobeha.2017.10.007

Power, Y., Goodyear, B., & Crockford, D. (2012). Neural correlates of pathological gamblers preference for immediate rewards during the Iowa gambling task: An fMRI study. *Journal of Gambling Studies*, 28(4), 623–636. https://doi.org/10.1007/s10899-011-9278-5

Preuschoff, K., Quartz, S. R., & Bossaerts, P. (2008). Human insula activation reflects risk prediction errors as well as risk. *Journal of Neuroscience*, 28(11), 2745–2752. https://doi.org/10.1523/jneurosci.4286-07.2008

Raghuraman, A. P., & Padoa-Schioppa, C. (2014). Integration of multiple determinants in the neuronal computation of economic values. *Journal of Neuroscience*, 34(35), 11583–11603. https://doi.org/10.1523/jneurosci.1235-14.2014

Rivalan, M., Coutureau, E., Fitoussi, A., & Dellu-Hagedom, F. (2011). Inter-individual decision-making differences in the effects of cingulate, orbitofrontal, and prelimbic cortex lesions in a rat gambling task. *Frontiers in Behavioral Neuroscience*, 5, 22. https://doi.org/10.3389/fnbeh.2011.00022

Rodriguez, C. A., Turner, B. M., & McClure, S. M. (2014). Intertemporal choice as discounted value accumulation. *PLoS One*, 9(2), e90138. https://doi.org/10.1371/journal.pone.0090138

Rolls, E. T. (2021). The neuroscience of emotional disorders. *Handbook of Clinical Neurology*, 183, 1–26. https://doi.org/10.1016/B978-0-12-822290-4.00002-5

Rolls, E. T., Joliot, M., & Tzourio-Mazoyer, N. (2015). Implementation of a new parcellation of the orbitofrontal cortex in the automated anatomical labeling atlas. *NeuroImage*, 122, 1–5. https://doi.org/10.1016/j.neuroimage.2015.07.075

Rose, E. J., Greene, C., Kelly, S., Morris, D. W., Robertson, I. H., Fahey, C., Jacobson, S., O'Doherty, J., Newell, F. N., McGrath, J., Bokde, A., Garavan, H., Frodl, T., Gill, M., Corvin, A. P., & Donohoe, G. (2012). The NOS1 variant rs6490121 is associated with variation in prefrontal function and grey matter density in healthy individuals. *NeuroImage*, 60(1), 614–622. https://doi.org/10.1016/j.neuroimage.2011.12.054

Schoenbaum, G., Chiba, A. A., & Gallagher, M. (1998). Orbitofrontal cortex and basolateral amygdala encode expected outcomes during learning. *Nature Neuroscience*, 1(2), 155–159. https://doi.org/10.1038/407

Schuck, N. W., Cai, M. B., Wilson, R. C., & Niv, Y. (2016). Human orbitofrontal cortex represents a cognitive map of state space. *Neuron*, 91(6), 1402–1412. https://doi.org/10.1016/j.neuron.2016.08.019

Siegel, J. S., Power, J. D., Dubis, J. W., Vogel, A. C., Church, J. A., Schlaggar, B. L., & Petersen, S. E. (2014). Statistical improvements in functional magnetic resonance imaging analyses produced by censoring high-motion data points. *Human Brain Mapping*, 35(5), 1981–1996. https://doi.org/10.1002/hbm.22307

St Onge, J. R., & Floresco, S. B. (2010). Prefrontal cortical contribution to risk-based decision making. *Cerebral Cortex*, 20(8), 1816–1828. https://doi.org/10.1093/cercor/bhp250

Stalnaker, T. A., Cooch, N. K., & Schoenbaum, G. (2015). What the orbitofrontal cortex does not do. *Nature Neuroscience*, 18(5), 620–627. https://doi.org/10.1038/nn.3982

Stark, C. E. L., Okado, Y., & Loftus, E. F. (2010). Imaging the reconstruction of true and false memories using sensory reactivation and the misinformation paradigms. *Learning & Memory*, 17(10), 485–488. https://doi.org/10.1101/lm.1845710

Stolyarova, A., & Izquierdo, A. (2017). Complementary contributions of basolateral amygdala and orbitofrontal cortex to value learning under uncertainty. *eLife*, 6, e27483. https://doi.org/10.7554/eLife.27483

Stuphorn, V. (2020). Decision making: How is information represented in orbitofrontal cortex? *Current Biology*, 30(1), R35–R37. https://doi.org/10.1016/j.cub.2019.11.015

Sutton, R. S., & Barto, A. G. (1998). *Reinforcement learning: An introduction*. MIT Press.

Suzuki, S., Cross, L., & O'Doherty, J. P. (2017). Elucidating the underlying components of food valuation in the human orbitofrontal cortex. *Nature Neuroscience*, 20(12), 1780–1786. https://doi.org/10.1038/s41593-017-0008-x

Tanabe, J., Reynolds, J., Krmpotich, T., Claus, E., Thompson, L. L., Du, Y. P., & Banich, M. T. (2013). Reduced neural tracking of prediction error in substance-dependent individuals. *American Journal of Psychiatry*, 170(11), 1356–1363. https://doi.org/10.1176/appi.ajp.2013.12091257

Tanabe, J., Thompson, L., Claus, E., Dalwani, M., Hutchison, K., & Banich, M. T. (2007). Prefrontal cortex activity is reduced in gambling and nongambling substance users during decision-making. *Human Brain Mapping*, 28(12), 1276–1286. https://doi.org/10.1002/hbm.20344

Tom, S. M., Fox, C. R., Trepel, C., & Poldrack, R. A. (2007). The neural basis of loss aversion in decision-making under risk. *Science*, 315(5811), 515–518. https://doi.org/10.1126/science.1134239

Verharen, J., Danner, U. N., Schröder, S., Aarts, E., van Elburg, A. A., & Adan, R. A. H. (2019). Insensitivity to losses: A Core feature in patients with anorexia nervosa? *Biological Psychiatry-Cognitive Neuroscience and Neuroimaging*, 4(11), 995–1003. https://doi.org/10.1016/j.bpsc.2019.05.001

Vertechi, P., Lottem, E., Sarra, D., Godinho, B., Treves, I., Quendera, T., Oude Lohuis, M. N., & Mainen, Z. F. (2020). Inference-based decisions in a hidden state foraging task: Differential contributions of prefrontal cortical areas. *Neuron*, 106(1), 166–176.e6. https://doi.org/10.1016/j.neuron.2020.01.017

Von Siebenthal, Z., Boucher, O., Rouleau, I., Lassonde, M., Lepore, F., & Nguyen, D. K. (2017). Decision-making impairments following insular and medial temporal lobe resection for drug-resistant epilepsy. *Social Cognitive and Affective Neuroscience*, 12(1), 128–137. https://doi.org/10.1093/scan/nsw152

Wallis, J. D. (2011). Cross-species studies of orbitofrontal cortex and value-based decision-making. *Nature Neuroscience*, *15*(1), 13–19. https://doi.org/10.1038/nn.2956

Wang, Y., Ma, N., He, X., Li, N., Wei, Z., Yang, L., Zha, R., Han, L., Li, X., Zhang, D., Liu, Y., & Zhang, X. (2017). Neural substrates of updating the prediction through prediction error during decision making. *NeuroImage*, *157*, 1–12. https://doi.org/10.1016/j.neuroimage.2017.05.041

Wei, Z., Han, L., Zhong, X., Liu, Y., Zha, R., Wang, Y., Yang, L. Z., Bu, J., Song, H., Wang, W., Zhou, Y., Gao, P., & Zhang, X. (2018). Chronic nicotine exposure impairs uncertainty modulation on reinforcement learning in anterior cingulate cortex and serotonin system. *NeuroImage*, *169*, 323–333. https://doi.org/10.1016/j.neuroimage.2017.11.048

Werner, N. S., Schweitzer, N., Meindl, T., Duschek, S., Kambeitz, J., & Schandry, R. (2013). Interoceptive awareness moderates neural activity during decision-making. *Biological Psychology*, *94*(3), 498–506. https://doi.org/10.1016/j.biopsycho.2013.09.002

Wilson, R. C., Takahashi, Y. K., Schoenbaum, G., & Niv, Y. (2014). Orbitofrontal cortex as a cognitive map of task space. *Neuron*, *81*(2), 267–279. https://doi.org/10.1016/j.neuron.2013.11.005

Xie, Y., Nie, C., & Yang, T. (2018). Covert shift of attention modulates the value encoding in the orbitofrontal cortex. *eLife*, *7*, e31507. https://doi.org/10.7554/eLife.31507

Yamada, H., Louie, K., Tymula, A., & Glimcher, P. W. (2018). Free choice shapes normalized value signals in medial orbitofrontal cortex. *Nature Communications*, *9*, 162. https://doi.org/10.1038/s41467-017-02614-w

Yang, D. Y., Chi, M. H., Chu, C. L., Lin, C. Y., Hsu, S. E., Chen, K. C., Lee, I. H., Chen, P. S., & Yang, Y. K. (2019). Orbitofrontal dysfunction during the reward process in adults with ADHD: An fMRI study. *Clinical Neurophysiology*, *130*(5), 627–633. https://doi.org/10.1016/j.clinph.2019.01.022

Zeeb, F. D., & Winstanley, C. A. (2011). Lesions of the basolateral amygdala and orbitofrontal cortex differentially affect acquisition and performance of a rodent gambling task. *The Journal of Neuroscience*, *31*(6), 2197–2204. https://doi.org/10.1523/JNEUROSCI.5597-10.2011

Zeeb, F. D., & Winstanley, C. A. (2013). Functional disconnection of the orbitofrontal cortex and basolateral amygdala impairs acquisition of a rat gambling task and disrupts animals' ability to alter decision-making behavior after reinforcer devaluation. *Journal of Neuroscience*, *33*(15), 6434–6443. https://doi.org/10.1523/jneurosci.3971-12.2013

Zha, R., Bu, J., Wei, Z., Han, L., Zhang, P., Ren, J., Li, J. A., Wang, Y., Yang, L., Vollstädt-Klein, S., & Zhang, X. (2019). Transforming brain signals related to value evaluation and self-control into behavioral choices. *Human Brain Mapping*, *40*(4), 1049–1061. https://doi.org/10.1002/hbm.24379

Zha, R., Tao, R., Kong, Q., Li, H., Liu, Y., Huang, R., Wei, Z., Hong, W., Wang, Y., Zhang, D., Fallgatter, A., Yang, Y., Zhang, X., Liang, P., & Rao, H. (2022). Impulse control differentiates internet gaming disorder from non-disordered but heavy internet gaming use: Evidence from multiple behavioral and multimodal neuroimaging data. *Computers in Human Behavior*, *130*, 107184. https://doi.org/10.1016/j.chb.2022.107184

Zhou, J., Gardner, M., & Schoenbaum, G. (2021). Is the core function of orbitofrontal cortex to signal values or make predictions? *Current Opinion in Behavioral Sciences*, *41*, 1–9. https://doi.org/10.1016/j.cobeha.2021.02.011

SUPPORTING INFORMATION

Additional supporting information may be found in the online version of the article at the publisher's website.